Advances in Atmospheric Sciences
Impact Factor: 3.158
E-alert
ISSN 0256-1530
CN 11-1925/O4

Observations of Dynamic Turbulence in the Lower Stratosphere over Inner Mongolia Using a High-resolution Balloon Sensor Constant Temperature Anemometer

Xiaoyu REN, Yi LIU, Zhaonan CAI, Yuli ZHANG

Citation: Ren, X. Y., Y. Liu, Z. N. Cai, Y. L. Zhang, 2022: Observations of Dynamic Turbulence in the Lower Stratosphere over Inner Mongolia Using a High-resolution Balloon Sensor Constant Temperature Anemometer, *Adv. Atmos. Sci.*, In press. doi: 10.1007/s00376-021-1233-5.

View online: https://doi.org/10.1007/s00376-021-1233-5

ADVANCES IN ATMOSPHERIC SCIENCES, VOL. 39, MARCH 2022, 519–528

• Notes & Letters •

Observations of Dynamic Turbulence in the Lower Stratosphere over Inner Mongolia Using a High-resolution Balloon Sensor Constant Temperature Anemometer

Xiaoyu REN[1,2], Yi LIU[1,2], Zhaonan CAI*[1], and Yuli ZHANG[1]

[1]*Carbon Neutrality Research Center*, *Institute of Atmospheric Physics*, *Chinese Academy of Sciences*, *Beijing* 100029, *China*

[2]*University of Chinese Academy of Sciences*, *Beijing* 100049, *China*

(Received 17 June 2021; revised 29 September 2021; accepted 26 October 2021)

ABSTRACT

We present characterizations of the dynamic turbulence in the lower stratosphere measured by a new balloon-based system designed for detecting finer scale dynamic turbulence. The balloon-based system included a constant temperature anemometer (CTA) operating at a sampling rate of 2 kHz at an ascent speed of 5 m s^{-1} (corresponding to a vertical resolution of 2.5 mm), an industrial personal computer, batteries, sensors for ambient temperature and humidity, an A/D converter, and others. The system was successfully launched to 24 km altitude over Bayannur City, Inner Mongolia Province. Results show the spatial intermittence of the turbulence layers, with clear boundaries between turbulent and non-turbulent regions. This is the first time that the dynamic turbulence spectrum down to the viscous sub-range has been obtained throughout the lower stratosphere over China. With that, the energy dissipation rates of dynamic turbulence could be calculated with high precision. The profile of the dissipation rates varied from 7.37×10^{-7} to 4.23 W kg^{-1} and increased with altitude in the stratosphere.

Key words: dynamic turbulence, stratosphere, balloon payload, high spatial resolution, dissipation rates, Inner Mongolia

Citation: Ren, X. Y., Y. Liu, Z. N. Cai, and Y. L. Zhang, 2022: Observations of dynamic turbulence in the lower stratosphere over Inner Mongolia using a high-resolution balloon sensor constant temperature anemometer. *Adv. Atmos. Sci.*, **39**(3), 519–528, https://doi.org/10.1007/s00376-021-1233-5.

Article Highlights:

- The dynamic turbulence in the stratosphere has been detected by the balloon system with the constant temperature anemometer (CTA) in China.
- The high-frequency CTA with a vertical spatial resolution of millimeters achieves the aim to observe small scale turbulence, leading to the turbulence energy spectrum down to the viscous sub-region.
- Vertical distribution characteristics of turbulence layers and the energy dissipation rates are more obvious. The turbulence layers appear intermittently in space and the rates of the energy dissipation increase with altitude.

1. Introduction

The stratosphere plays an important role in weather forecasting and climate research. For example, it couples the upper and lower layers of the atmosphere via waves on various scales (Lv et al., 2009). Gravity waves can transport a large amount of energy upward and their amplitude increases with height as the air density decreases (Moldovan et al., 2002; Costantino et al., 2015). The gravity waves break because of the atmosphere instability, such as the dynamic instability, or the temperature gradient exceeding the adiabatic lapse rate. The breaking gravity waves can generate turbulence and secondary gravity waves. Then the dynamic energy of turbulence cascades until it dissipates into heat. As a result, the energy fluxes in the stratosphere are altered and trace species are mixed. It is therefore important to study dynamic turbulence in the stratosphere to quantify the energy budget and the mixing of trace species (Lilly et al., 1974). Stratospheric turbulence is also important for aviation (Dutton, 1971; Kim and Chun, 2011) and its accurate prediction is the key to aviation safety. Research on stratospheric turbulence has provided important theoretical and practical values.

Turbulence dissipates on the scale of centimeters or smaller. Previous research has shown that higher spatial resolution gives more accurate turbulence parameters (Lübken et al., 1993; Wilson et al., 2011), leading to challenging technical requirements for the instruments. Another difficulty is that the frequency of the occurrence of turbulence in the stra-

* Corresponding author: Zhaonan CAI
Email: caizhaonan@mail.iap.ac.cn

tosphere is less than that in the troposphere and the atmospheric boundary layer, because the stratospheric layers are relatively stable (Lübken, 1992). In addition, because the altitude of the stratosphere is higher, this makes the detection more difficult. Stratospheric turbulence is, therefore, less well studied and understood than turbulence in the lower atmosphere.

Several approaches have been applied to the research on stratospheric turbulence. These research methods fall into two main categories: instrumental detection and numerical models. There are two types of detection methods that can be used in the stratosphere: remote sensing and in situ soundings. Remote sensing methods (e.g., radar systems and satellites) give continuous detection, but their spatial resolution is relatively coarse (Sato et al., 1985; Gibson et al., 2007). In situ soundings use aircraft, rockets, or balloons to carry the detection instruments. Aircraft have been used to study the clear-air turbulence at 12–15 km altitude since the 1960s (Waco, 1970). These experiments showed the intermittence of the clear-air turbulence and its relationship with the Richardson number but limited in height. Rockets passing through the stratosphere and into the upper mesosphere (Lübken et al., 2002) can be used to show the source of turbulence and the relationship with the background atmosphere. Although these methods have been used to detect turbulence, there are difficulties to detect small-scale turbulence in the stratosphere. In situ balloon soundings with high-resolution sensors can be used to study the fine structure of stratospheric turbulence and can be carried to specified atmospheric heights in different regions (Barat et al., 1984). Our research objectives are to obtain the parameters and spatial distribution of stratospheric turbulence by conducting experiments at a high spatial resolution with high vertical resolution.

Numerical studies include direct numerical simulations (Fritts and Wang, 2013), weather research and forecasting simulations (Schneider et al., 2017), and large-eddy simulations (Dupuy et al., 2019). These models are useful tools to study turbulence, but their limitations include low accuracy and coarse resolution. Additional problems include a lack of understanding of the source and characteristics of the turbulence. To help deal with these problems, it is necessary to conduct extensive field experiments in the stratosphere (Gavrilov et al., 2005).

Dynamic turbulence is one of the important aspects in turbulence studies. Turbulence is manifested in two forms: temperature fluctuations and wind fluctuations. Temperature fluctuations in the stratosphere influence astronomical observations and communication (Wu et al., 2007). However, dynamic turbulence is detected less often than turbulence in the temperature field. One of the main reasons for this is that the wind field is a vector quantity, and the wind direction should also be considered. This requires a higher instrument sensitivity and difficult techniques. However, dynamic turbulence cannot be overlooked because wind fluctuations are the direct manifestation of turbulent motion. Wind fluctuations influence the dynamic mechanism of the flow field, resulting in changes in the temperature field (Theuerkauf, 2012).

We describe the detection of dynamic turbulence in the lower stratosphere referring to the concepts proposed by the Leibniz Institute of Atmospheric Physics (Theuerkauf et al., 2011). This is the first time that in-situ turbulence observations with sub-centimeter spatial resolution were carried out in China. We used a constant temperature anemometer (CTA) for the detection of anomalies of wind speed in the stratosphere. The CTA measures wind fluctuations at a high frequency (kHz), resulting in a vertical spatial resolution at the millimeter scale. Our system offers the possibility of studying the dynamic turbulence spectrum down to the viscous sub-range in the stratosphere. The dissipation scale of the stratospheric turbulence can be as small as millimeters, below which the turbulent mechanical energy of small-scale vortexes is converted to heat. The dissipation rate is the primary parameter used to quantify the effect of turbulence in the stratosphere (Dole and Wilson, 2001). The higher spatial resolution of the CTA allows us to obtain more accurate energy dissipation rates and identify thinner layers of turbulence over the whole vertical profile.

This paper presents details of our experiments and the obtained results. Section 2 describes the design of the system and the experimental procedure. Section 3 presents the observation signals, the characteristics of the turbulence layers and the turbulence parameters. Section 4 discusses the calibration method and consequences, and Section 5 summarizes our results and future research plans.

2. Experimental methods

There are few published observations of the sub-centimeter-scale dynamic turbulence in the stratosphere. Lübken and coworkers used CTA sensors to resolve the targets for high spatial resolution observations (Haack et al., 2014; Schneider et al., 2017) and we aimed to apply this technique in China.

We designed an in situ experimental system to measure fluctuations in the wind field. Figure 1 shows a schematic drawing of the principle of our balloon sensor system and photographs of the experimental site. The payload of the system includes the CTA, the batteries, an A/D converter, an industrial personal computer, and a 3-axis gyroscope. The CTA is the main instrument consisting of CTA probes and bridges. The platinum-plated tungsten wires of the CTA probes are 5 μm in diameter and 1.25 mm in length. The wires are placed vertically, parallel to the vertical wind, which means that the probes are most sensitive to horizontal winds and least sensitive to vertical winds. The supports of the probes are placed 20 cm above the top of the payload to reduce the impact of the payload wake. The CTA has a vertical spatial resolution of 2.5 mm with a sampling frequency of 2 kHz at an ascent rate of 5 m s^{-1} (The actual ascent speed changes little with altitude, with

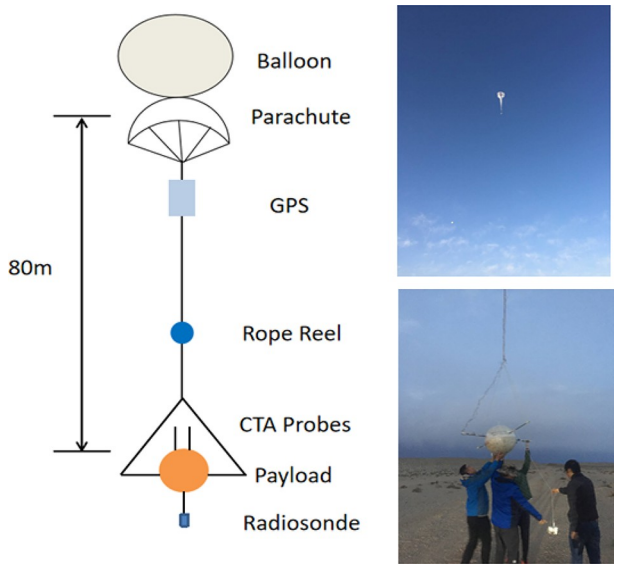

Fig. 1. Schematic drawing of the principle of the balloon sensor dynamic turbulence system and photographs of the site of the experiment.

the average ascent rate being 4.85 m s^{-1}.).

The CTA bridges are a kind of Wheatstone bridge. The voltage signals change with the convective cooling caused by the airflow passing the hot wire. The output signals of the bridges are converted by the 16-bit NI-ADC and the voltage signals output by the A/D converter are recorded and saved in the industrial personal computer. The 3-axis gyroscope measures the rotation and pendulum of the payload. These instruments and the batteries are placed in the payload, which is a Styrofoam box providing both thermal insulation and protection to the instruments from impact with the ground. The payload is spherical, which gives a calmer flight than a square box according to Schneider's test (Schneider, 2015). A radiosonde with a sampling resolution of 1 s is hung 6 m below the payload to provide background atmospheric profiles (e.g., temperature, wind speed, wind direction, pressure, and humidity).

The payload is launched with a zero-pressure balloon and therefore some of the measurements should follow the principles of balloon sounding. The distance between the balloon and the payload is 80 m, sufficiently far that the payload is little influenced by the balloon wake. However, this long-distance causes difficulties at the launch. A rope reel is required to roll up most of the rope. The rope is released from the reel after the successful lift-off of the payload. The CTA probes are very fragile, so preparations for the launch need to be careful and steady. After the balloon has inflated, it is tied to the vehicular automatic winding machine with a string. The string is released to let the balloon rise slowly and is then cut when the payload hangs smoothly in the air. The balloon can float horizontally for some distance when the payload reaches a specific altitude, allowing measurements of the horizontal distribution of the stratospheric turbulence. The rope connecting the payload to the balloon is then cut. The parachute opens automatically after a few seconds to slow the descent of the payload. Throughout the experiment, GPS is used to continuously pinpoint the location of the balloon to confirm the final landing point. The system with the observational data is then recovered and can be used again.

3. Observations of turbulence

3.1. *Time series of signal fluctuations*

We successfully carried out experiments in Bayannur City, Inner Mongolia Province, China (41°N, 108°E) in November 2019. Figure 2 shows the flight trajectory. The balloon system rose vertically to 24 km altitude. We obtained voltage signals and the corresponding radiosonde profile over the whole range of altitude. The voltage signals were used to study the stratospheric turbulence and the reasons were described in section 4. The pendulum effect and rotation of the payload produced a series of low-frequency signals superimposed on the turbulence signals, and these large-scale trends needed to be filtered out to obtain the fluctuations of dynamic turbulence. We first removed the trend spline from the signals by the moving window with the length of low-frequency motion and then identified the turbulence and non-turbulence layers (Haack et al., 2014). Figure 3 shows many turbulence layers (red dots) over the whole profile identified by the cluster algorithm that there are at least n turbulent points within distance d. The thickness of the turbulence layers varies from a few hundred meters to a few meters with altitude and the spatial intermittence is significant over the entire altitude range.

Figure 4 shows the voltage signals for altitudes between 16.74 and 16.86 km. The left-hand panel presents the raw data in blue, and then the spline trend in black was subtracted from the raw data. The results for the wind fluctuations are shown in the right-hand panel. The region has three turbulence layers: L1 between 16.822 km and 16.844 km; L2 between 16.81 km and 16.815 km; and L3 between 16.75 km and 16.805 km. The layers are separated by calm regions with clear boundaries. The thickness of the three layers varies greatly. These results show that the CTA system can observe turbulence layers with different thicknesses including the thin layers of a few meters.

3.2. *Spectral analysis*

The turbulence energy spectrum is a useful tool with which to study stratospheric turbulence and shows how much turbulence vortices at different scales contribute to the energy spectrum (Theuerkauf, 2012). The energy spectrum is divided into three parts: the buoyancy sub-range, the inertial sub-range, and the viscous sub-range. Some wave motions are superimposed on the turbulence at the scale of the buoyancy and partial inertial sub-range. Because it is difficult to separate these motions from the turbulence, we therefore focused on small-scale vortices in the inertial and viscous sub-ranges.

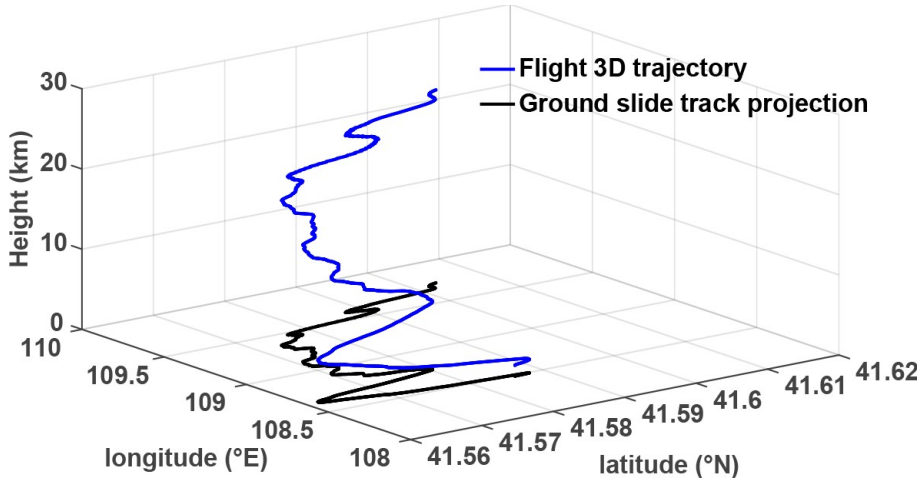

Fig. 2. Trajectory of the payload during ascent. The blue line shows the 3D trajectory and the black line shows the ground projection of the 3D trajectory.

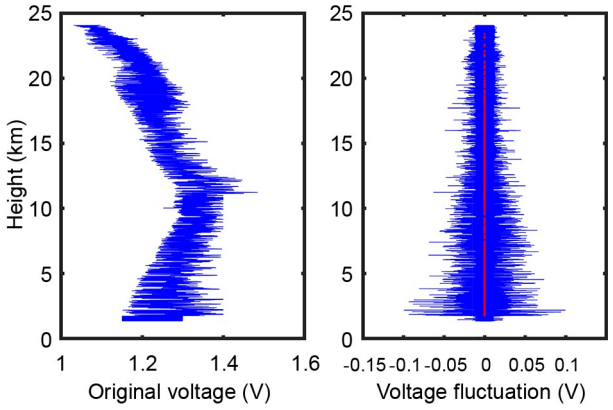

Fig. 3. Left-hand panel: profile of original velocity during the flight. Right-hand panel: profile of velocity fluctuation (blue) and turbulence layer (red).

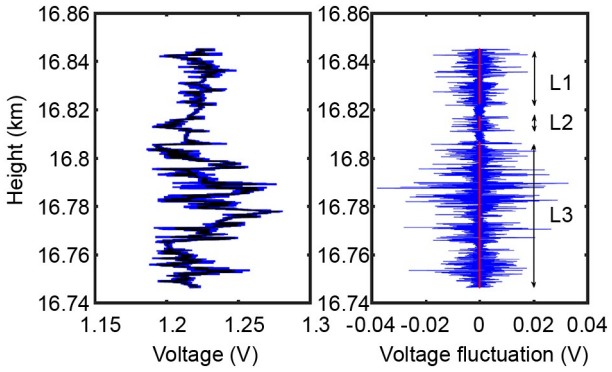

Fig. 4. Example of the observed profiles of velocity fluctuations between 16.74 and 16.86 km. Regions with strong turbulent fluctuations (red) can be clearly distinguished from calm regions.

The CTA system gives a millimeter-scale spatial resolution in the stratosphere and the spectrum down to the partial viscous sub-region. We use the inner scale l_0 to describe the transition between the viscous sub-ranges and inertial sub-ranges. If the scale is smaller than l_0, then the turbulence energy is dissipated into heat and changes the energy flux. The energy dissipation rate is used to estimate the influence of turbulence on the stratosphere (Kantha and Hocking, 2011).

We used the Welch method, which uses the periodogram method based on the fast Fourier transform, to calculate the power spectral density (PSD) (Welch, 1967). This method divides the data into N partially overlapping segments and then a window function is used to estimate the spectral density of each segment. The spectra of all segments are then averaged. This method is effective in reducing the variance and deviation of power spectra, leading to better estimations.

The spectrum of turbulence layer L3 (in Fig. 3) is shown in Fig. 5 by the blue line. The horizontal axis of spatial scales is calculated from the formula $L = 2\pi/k = v_b/f$, where k is the wave-number, f is the sampling frequency and v_b is the velocity of the balloon. The slopes of two solid lines are −5/3 and −7 respectively. The middle part of the PSD curve (in blue) paralleling the orange line (−5/3 slope) is the inertial sub-range. The partial tail paralleling the yellow line (−7 slope) is the viscous sub-range. These results are in great agreement with the Kolmogorov −5/3 theory (Tennekes and Lumley, 1972). The PSD does not decrease continuously in the tail due the instrument noise. These experimental data therefore cover the inertial sub-ranges and partial viscous sub-ranges. The inner scale, below which the turbulence energy begins dissipating into heat, can therefore be resolved.

In addition, the non-turbulence region, for example, between 16.805–16.810 km has also been calculated as above. Compared with the spectrum of the turbulence region, Fig. 6 shows the spectrum does not follow the slope of −3/5 in the inertial sub-range. The power spectral densities are much smaller than for the turbulence case and close to the noise level. Given the above, the Welch method is a useful way to calculate PSD for the further study.

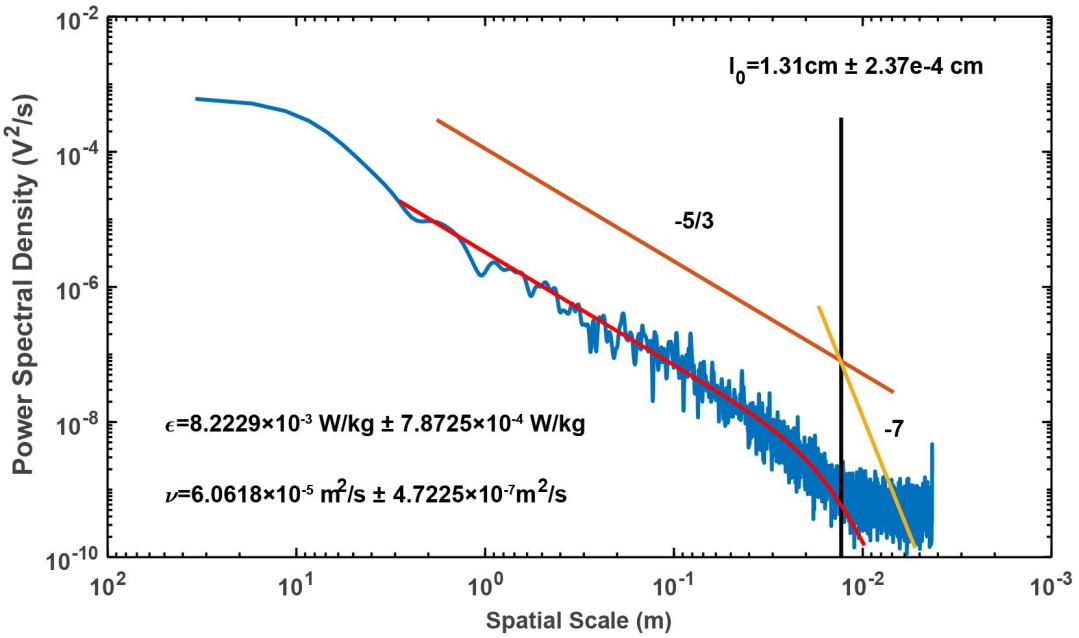

Fig. 5. Power spectral density of the voltage fluctuations for a turbulence region (16.75–16.805 km). The red curve shows the fit of the Heisenberg model to the measured spectrum. The black line indicates the inner scale l_0. The errors of l_0, υ and ε are ±2.37×10^{-4} cm, ±4.7225×10^{-7} m^2 s^{-1} and ±7.8275×10^{-4} W kg^{-1} respectively.

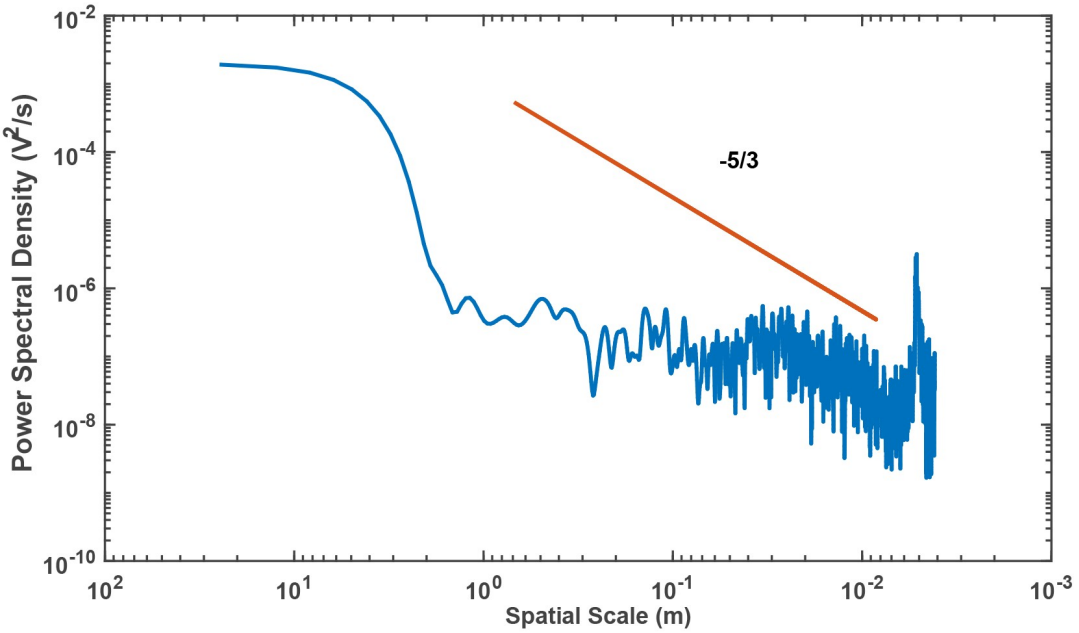

Fig. 6. Power spectral density of the voltage fluctuations for a non-turbulence region (16.805–16.810 km).

3.3. *Calculation of the energy dissipation rate*

The energy dissipation rate represents the rate at which the turbulence energy is dissipated into heat. To retrieve the energy dissipation rate, Heisenberg (1948) proposed a fitting model for which the density fluctuations have a slope of −5/3 in the inertial sub-range and −7 in the viscous sub-range. This method has been applied to rocket explorations by Lübken (1992). The method has also been applied to balloon observations since 2011 (Theuerkauf et al., 2011). Based on the Heisenberg model, the first step is to fit the theoretical model to the measured spectrum:

$$W(\omega) = \frac{\Gamma(5/3)\sin(\pi/3)}{2\pi v_b} C_v^2 \frac{(\omega/v_b)^{-5/3}}{\{1+[(\omega/v_b)/k_0]^{8/3}\}^2}, \quad (1)$$

where Γ is the gamma function ($\Gamma(5/3) = 0.90167$), $\omega = 2\pi f$ is the cyclic frequency and C_v^2 is the structure function. l_0 can then be obtained from the best fit, which is directly

related to the rate of dissipation ε:

$$l_0 = 5.7\left(\frac{\upsilon^3}{\varepsilon}\right)^{1/4}, \quad (2)$$

where υ is the kinematic viscosity calculated from the radiosonde data. For example, the red line in Fig. 5 is the best-fit result of the turbulence spectrum that corresponds to $W(\omega)$ in Eq. (1) and gives l_0=(1.31±2.37)×10^{-4} cm (fit error). The inertial sub-range extends from a spatial scale of 7 m to 0.02 m, while the viscous sub-range falls below a spatial scale of 0.02 m. The instrument noise is 10^{-9} V^2 s^{-1} below the 10^{-2} m spatial scale. The rate of energy dissipation (8.22 mW kg^{-1} ±7.8275×10^{-4} W kg^{-1}) is calculated from Eq. (2).

3.4. *Profile of energy dissipation rate*

The first step in obtaining the vertical distribution of the dissipation rates in the stratosphere is to identify the turbulence layers in the vertical profile. The velocity fluctuation data are divided into segments of scale ~20 m (4 seconds with the rate of ascent ~5 m s^{-1}) with the overlap of 10 m. The spectra of every segment are calculated. Then judging whether it is the turbulent spectrum as mentioned in Section 3.2, the energy dissipation rates are obtained by fitting the turbulent spectra. The energy dissipation rates of the non-turbulent regions are set to zero. The profile of the rate of dissipation is finally obtained. The points in Fig. 7 shows that the dissipation rates range from 7.37×10^{-7} W kg^{-1} at 7.41 km to 4.23 W kg^{-1} at 18.45 km. The red line is the semi-logarithmic linear regression line showing that the overall trend of the dissipation rates increases with height.

The dissipation rates as a function of height cover several orders of magnitude. Therefore, the profile is divided into three height ranges for further study. The left-hand panel in Fig. 8 shows the dissipation rate at 7–14 km, the middle panel at 14–20 km, and the right-hand panel at 20–24 km. Because the dissipation rates vary by a few orders of magnitude, the three panels have different height ranges and different scales on the x-axis. The large and small values (including the zero values) of the dissipation rates alternate, suggesting that the areas of turbulence and laminar flow alternate with height.

The results are consistent with the theory of turbulence space intermittency throughout the profile. The left-hand panel shows that the values of dissipation rates are small, but the number of layers of turbulence is largest at 7–14 km. There are some clear layers of turbulence at about 7.1 km, 8.4 km, 10.7 km, 11.1 km, 12 km, 12.5 km, 13 km and 13.5 km altitude. The layers of small dissipation rates appear intermittently between the layers of larger dissipation rates, and it is hard to find layers of non-turbulence in this region of the stratosphere. The dissipation rates are relatively large at 14–20 km, but the number of turbulent layers decreases. There are a few clear turbulence layers at about 16 km, 17.6 km, 18.4 km and 19.1 km altitude. At 20–24 km, although the dissipation rates increase with height, the number of turbulence layers is less especially at 23–24 km. There are clear layers of turbulence with the highest rate of energy dissipation at 21.5–22 km altitude. In summary, the dissipation rates increase with height and the profile clearly shows the intermittence in stratospheric turbulence.

The dissipation rates range from 1×10^{-7} to 1×10^{0} W kg^{-1}. The result is similar to the findings of Lübken et al. (2002) and Schneider et al. (2017), but it is larger than obtained from balloon flights in the 1980s, when the values were

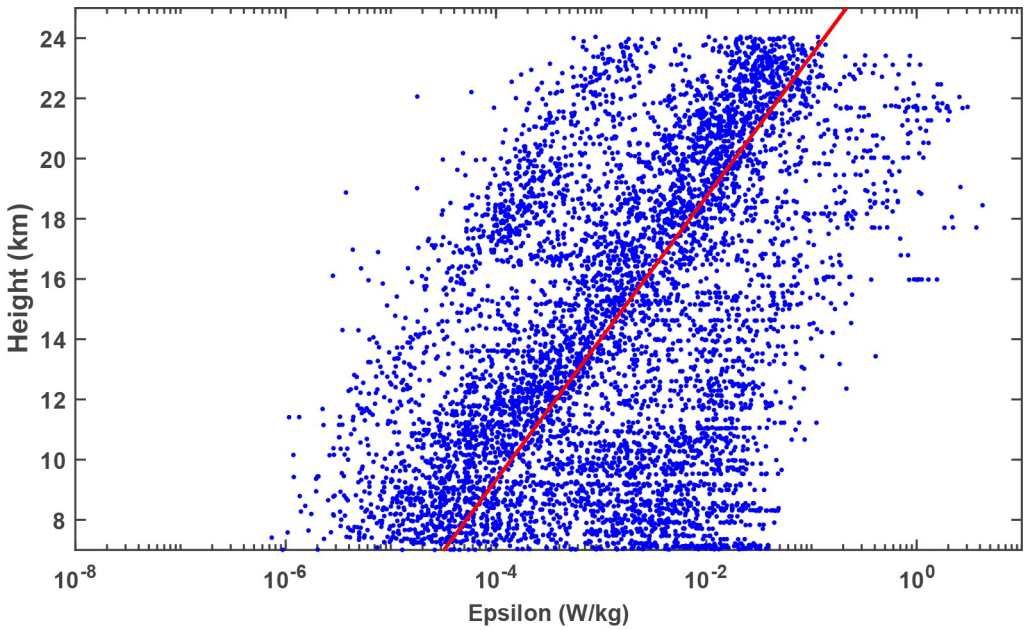

Fig. 7. Rate of energy dissipation (blue) plotted on a semi-logarithmic scale against the height between 7 and 24 km. The red line shows the linear regression of the log dissipation rate.

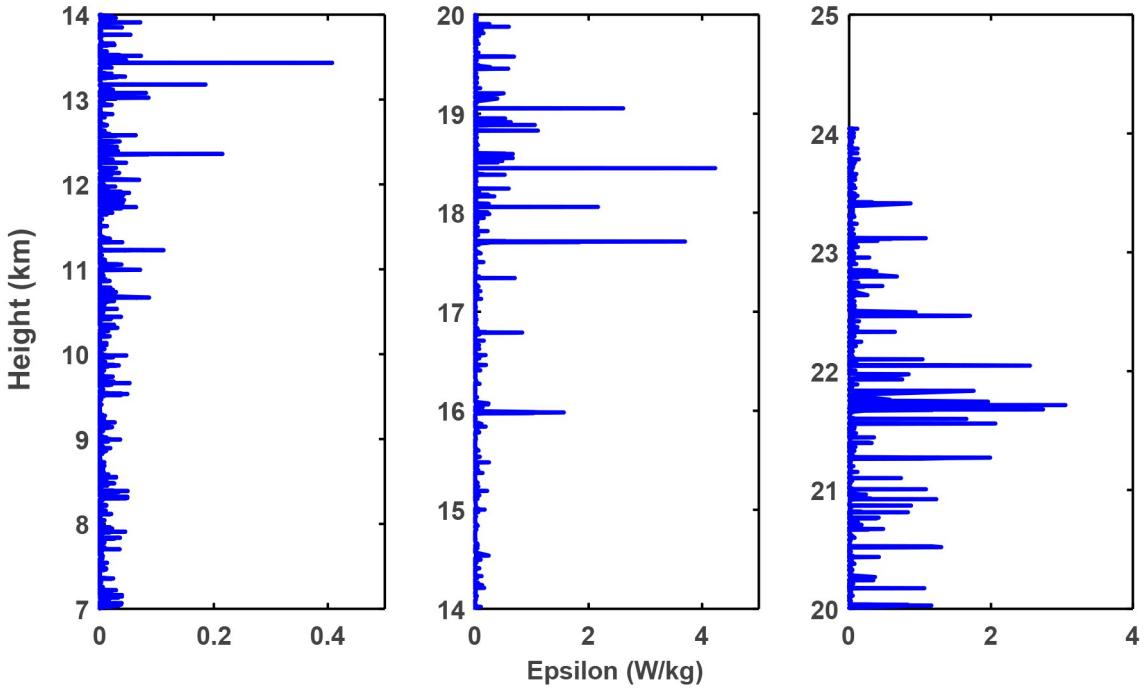

Fig. 8. Profile of the rate of dissipation on a linear scale divided into three altitude segments (left-hand, middle and right-hand panels). Note that since the dissipation rates vary by a few orders of magnitude, the three panels have different height ranges and different scales on the *x*-axis.

between 1×10^{-5} and 5×10^{-5} W kg^{-1} (Barat, 1982; Barat and Bertin, 1984). We suggest the reason for the discrepancy is the difference of observed objections, research events and sensors. Some dissipation rates in 1970s–80s were calculated with the temperature fluctuations, which either decreased or were constant with height (Schneider, 2015). Also, clear-air turbulence was included in the analysis of the profiles, so there were small changes in values of the dissipation rates. Moreover, different sensors and computation methods may also result in some discrepancies.

4. Vicarious calibration discussion

Changes in the background temperature and pressure affect the response of the CTA and therefore the probes need to be calibrated. Note that the relative humidity in the stratosphere is so low that its influence can be ignored. The calibration experiment was previously carried out in climate and vacuum laboratories by the Leibniz Institute of Atmospheric Physics (Theuerkauf et al., 2011). We use the same type of CTA probes and bridges as the Leibniz Institute of Atmospheric Physics. We carried out the calibration tests at normal pressure and temperature, similar to the conditions of 20°C and 1000 hPa used by Theuerkauf et al. (2011). It is therefore reasonable to refer to their results of the calibration experiment. Their data calibration was performed by interpolating the wind values to the same frequency as the CTA data and then normalizing the velocity fluctuations to the corrected voltage fluctuations based on the sensitivity curves. Their results showed that the corrected voltage fluctuations were very similar to the measured voltage fluctuations, and they concluded that the uncorrected signals could be used directly to determine the turbulence parameters.

We verified these conclusions in a different way: normalizing the voltage signals to the wind signals at 2000 Hz. The first step was to average the voltage signals from 2000 to 1 Hz to obtain the coefficients $k_i = \text{voltage}_{\text{mean}\,i}/\text{velocity}_i$. The corrected wind signals at 2000 Hz were obtained from $\text{velocity}_{\text{corrected}} = \text{voltage}_{\text{measured}} k_i$ (left-hand panel of Fig. 9) , and the fluctuations in the corrected velocity are obtained (right-hand panel of Fig. 9). Fig. 10 shows some of the spectra for the high-frequency corrected velocities (in orange) and the measured voltages (in blue) at different

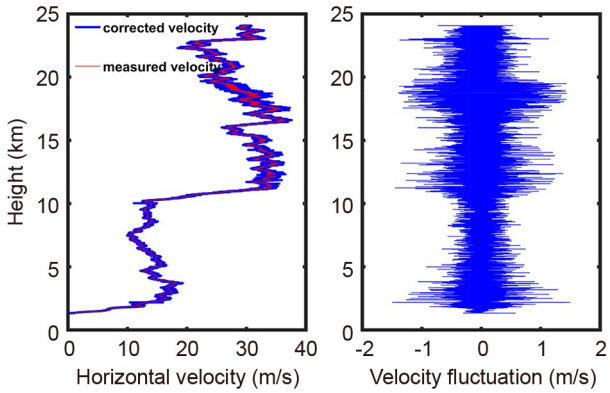

Fig. 9. Left-hand panel: profile of corrected (blue) and measured (red) velocity signals during the flight. Right-hand panel: profile of the corrected velocity fluctuations.

heights. The shapes of the corrected velocity fluctuations and measured voltage fluctuations are almost identical, but the PSDs differ by two to three orders of magnitude, i.e., the turbulence spectra shift up or down vertically. This movement is because the corrected velocity signals simply scale the absolute values of the turbulence fluctuations; in other words, the absolute values of the PSD change, but the shape shows little change. The dissipation rates only depend on the position of l_0 rather than the absolute values of the PSD, so the vertical shift as Fig. 10 has little effect on the value of l_0. There are deviations between the values of l_0 for the corrected and measured signals. This may be because k_i (1 Hz) is used as the coefficient for the corresponding 2000 Hz data, which produces small deviations in the corrected signals. The statistical results show that the average deviation of l_0 is 7%, giving an average error in the dissipation rate of 20%–30%. This margin of deviation is acceptable. To sum up, it is reasonable to use the voltage signals to replace the absolute wind signals.

5. Discussion and conclusions

We have presented a fine resolution dynamic turbulence observation system that was launched via balloon in Bayannur, Inner Mogolia on 20 November, 2019. The system can measure wind fluctuations in the lower stratosphere and can be used to determine high-resolution, millimeter-scale dynamic turbulence profiles from ground level up to the lower stratosphere. The system can detect layers of turbulence up to several hundred meters thick and also thinner layers of turbulence a few meters thick. The boundaries between the turbulence and non-turbulence layers are clear, and the spatial intermittency of the turbulence is obvious. To the best of our knowledge, this is the first successful high spatial resolution experiment in the stratosphere over China.

We obtained voltage fluctuations representing the dynamic turbulence by the Welch method. Our results showed that the slope of the spectra of the turbulence layers is −5/3 in the inertial sub-range and −7 in the viscous sub-range, which corresponds well with the Kolmogorov −5/3 power law. The spectra of the non-turbulence layers do not show these characteristics. Our results suggest that the voltage signals are valid dynamic fluctuation signals. The spectra cover the inertial sub-range and part of the viscous sub-region. The Heisenberg model is suitable for fitting the PSD in these sub-regions, thus, the inner scale could be determined.

One of our major research goals is to obtain the turbulence energy dissipation rate which depends only on the inner scale. The example of the turbulence spectrum shows that the inner scale of the turbulence layer at 16.81 km is 1.31 cm and its energy dissipation rate is 8.22 mW kg^{-1}. The dissipation rates over the entire height range were acquired to study the characteristics of the distribution. The minimum and maximum values of the dissipation rate points are 7.37×10^{-7} W kg^{-1} and 4.23 W kg^{-1} respectively. The values of the dissipation rates vary by several orders of magnitude and the over trend increases with height. The profile of the dissipation rates is divided into three parts: (1) the height range 7–14 km with the greatest number of turbulence layers and the smallest average value of the dissipation rates; (2) the height range 14–20 km with a moderate number of turbulence layers and a moderate average value of the dissipation rates; and (3) the height range 20–24 km with the lowest number of turbulence layers and the largest average value of the dissipation rates. The energy dissipation rates are higher in the stratosphere than in the upper tro-

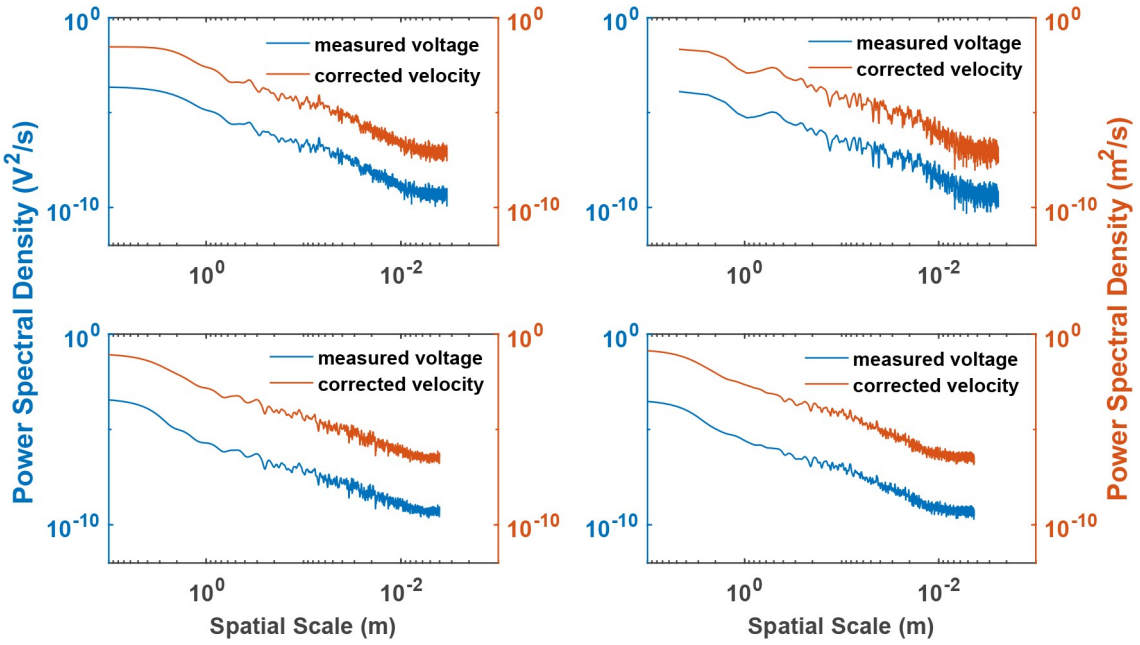

Fig. 10. Spectra of the measured (red) and corrected (blue) velocity signals at different heights.

posphere, meaning that the corresponding heating rates are higher in the stratosphere. This fact indicates that the dynamic turbulence has a potential influence on the energy budget and the mixing of trace species in the lower stratosphere.

These conclusions raise new questions such as the relationship with the atmospheric conditions and the statistical characteristics of the turbulence layers. The above results are drawn from the limited datasets, so more experiments are needed to explore the stratospheric turbulence for the future study. Moreover, the combination of observations with numerical simulations would be meaningful to study the source of turbulence.

Acknowledgements. This work was supported by the Strategic Priority Research Program of the Chinese Academy of Sciences (Grant No. XDA17010102). The authors thanks Prof. Mingyu ZHOU and Prof. Fei HU for their useful comments.

REFERENCES

Barat, J., 1982: Some characteristics of clear-air turbulence in the middle stratosphere. *J. Atmos. Sci.*, **39**(11), 2553–2564, https://doi.org/10.1175/1520-0469(1982)039<2553:SCOCAT>2.0.CO;2.

Barat, J., and F. Bertin, 1984: Simultaneous measurements of temperature and velocity fluctuations within clear air turbulence layers. Analysis of the estimate of dissipation rate by remote sensing techniques. *J. Atmos. Sci.*, **41**(9), 1613–1619, https://doi.org/10.1175/1520-0469(1984)041<1613:SMOTAV>2.0.CO;2.

Barat, J., C. Cot, and C. Sidi, 1984: On the measurement of the turbulence dissipation rate from rising balloons. *J. Atmos. Oceanic Technol.*, **1**(3), 270–275, https://doi.org/10.1175/1520-0426(1984)001<0270:OTMOTT>2.0.CO;2.

Costantino, L., P. Heinrich, N. Mzé, and A. Hauchecorn, 2015: Convective gravity wave propagation and breaking in the stratosphere: Comparison between WRF model simulations and Lidar data. *Annales Geophysicae*, **33**(9), 1155–1171, https://doi.org/10.5194/angeo-33-1155-2015.

Dole, J., and R. Wilson, 2011: Turbulence dissipation rates and vertical diffusivity in the stratosphere from radar observations. *Physics and Chemistry of the Earth, Part B: Hydrology, Oceans and Atmosphere*, **26**, 225–229, https://doi.org/10.1016/S1464-1909(00)00244-6.

Dupuy, D., A. Toutant, and F. Bataille, 2019: Study of the large-eddy simulation subgrid terms of a low Mach number anisothermal channel flow. *International Journal of Thermal Sciences*, **135**, 221–234, https://doi.org/10.1016/j.ijthermalsci.2018.09.001.

Dutton, J. A., 1971: Clear-air turbulence, aviation, and atmospheric science. *Rev. Geophys.*, **9**(3), 613–657, https://doi.org/10.1029/RG009i003p00613.

Fritts, D. C., and L. Wang, 2013: Gravity wave–fine structure interactions. Part II: Energy dissipation evolutions, statistics, and implications. *J. Atmos. Sci.*, **70**(12), 3735–3755, https://doi.org/10.1175/JAS-D-13-059.1.

Gavrilov, N. M., H. Luce, M. Crochet, F. Dalaudier, and S. Fukao, 2005: Turbulence parameter estimations from high-resolution balloon temperature measurements of the MUTSI-2000 campaign. *Annales Geophysicae*, **23**, 2401–2413, https://doi.org/10.5194/angeo-23-2401-2005.

Gibson, C. H., R. N. Keeler, V. G. Bondur, P. T. Leung, H. Prandke, and D. Vithanage, 2007: Submerged turbulence detection with optical satellites. *Proc. of SPIE 6680, Coastal Ocean Remote Sensing*, San Diego, SPIE, 114–119, https://doi.org/10.1117/12.732257.

Haack, A., M. Gerding, F.-J., and Lübken, 2014: Characteristics of stratospheric turbulent layers measured by LITOS and their relation to the Richardson number. *J. Geophys. Res.*, **119**(18), 10 605–10 618, https://doi.org/10.1002/2013JD021008.

Heisenberg, W., 1948: Zur statistischen theorie der turbulenz. *Zeitschrift für Physik*, **124**, 628–657, https://doi.org/10.1007/BF01668899.

Kantha, L., and W. Hocking, 2011: Dissipation rates of turbulence kinetic energy in the free atmosphere: MST radar and radiosondes. *Journal of Atmospheric and Solar-Terrestrial Physics*, **73**, 1043–1051, https://doi.org/10.1016/j.jastp.2010.11.024.

Kim, J.-H., and H.-Y. Chun, 2011: Statistics and possible sources of aviation turbulence over South Korea. *J. Appl. Meteor. Climatol.*, **50**(2), 311–324, https://doi.org/10.1175/2010JAMC2492.1.

Lilly, D. K., D. E. Waco, and S. I. Adelfang, 1974: Stratospheric mixing estimated from high-altitude turbulence measurements. *J. Appl. Meteor. Climatol.*, **13**, 488–493, https://doi.org/10.1175/1520-0450(1974)013<0488:SMEFHA>2.0.CO;2.

Lübken, F.-J., 1992: On the extraction of turbulent parameters from atmospheric density fluctuations. *J. Geophys. Res.*, **97**(D18), 20 385--20 395, https://doi.org/10.1029/92JD01916.

Lübken, F.-J., W. Hillert, G. Lehmacher, and U. Von Zahn, 1993: Experiments revealing small impact of turbulence on the energy budget of the mesosphere and lower thermosphere. *J. Geophys. Res.*, **98**(D11), 20 369–20 384, https://doi.org/10.1029/93JD02055.

Lübken, F.-J., M. Rapp, and P. Hoffmann, 2002: Neutral air turbulence and temperatures in the vicinity of polar mesosphere summer echoes. *J. Geophys. Res.*, **107**, 4273, https://doi.org/10.1029/2001JD000915.

Lv, D. R., and Coauthors, 2009: Frontiers and significance of research on stratospheric processes. *Advances in Earth Science*, **24**, 221–228, https://doi.org/10.3321/j.issn:1001-8166.2009.03.001. (in Chinese with English abstract)

Moldovan, H., F. Lott, and H. Teitelbaum, 2002: Wave breaking and critical levels for propagating inertio-gravity waves in the lower stratosphere. *Quart. J. Roy. Meteor. Soc.*, **128**(580), 713–732, https://doi.org/10.1256/003590002321042162.

Sato, T., T. Tsuda, S. Kato, S. Morimoto, S. Fukao, and I. Kimura, 1985: High-resolution MST observations of turbulence by using the MU radar. *Radio Sci.*, **20**(6), 1452–1460, https://doi.org/10.1029/RS020I006P01452.

Schneider, A., 2015: In-situ turbulence observations in the stratospheric wind and temperature field. . PhD dissertation, Universität Rostock.

Schneider, A., J. Wagner, J. Söder, M. Gerding, F.-J., and Lübken, 2017: Case study of wave breaking with high-resolution turbulence measurements with LITOS and WRF simulations. *Atmospheric Chemistry and Physics*, **17**, 7941–7954,

https://doi.org/10.5194/acp-17-7941-2017.

Tennekes, H., and J. L. Lumley, 1972: *A First Course in Turbulence*. MIT Press, 320 pp.

Theuerkauf, A., 2012: Stratospheric turbulence observations with the new balloon-borne instrument LITOS. PhD dissertation, Universitat Rostock.

Theuerkauf, A., M. Gerding, F.-J., and Lübken, 2011: LITOS-a new balloon-borne instrument for fine-scale turbulence soundings in the stratosphere. *Atmospheric Measurement Techniques*, **4**, 55–66, https://doi.org/10.5194/amt-4-55-2011.

Waco, D. E., 1970: A statistical analysis of wind and temperature variables associated with high altitude clear air turbulence (HICAT). *J. Appl. Meteor. Climatol.*, **9**(2), 300–309, https://doi.org/10.1175/1520-0450(1970)009<0300:ASAOWA>2.0.CO;2.

Welch, P., 1967: The use of fast Fourier transform for the estimation of power spectra: A method based on time averaging over short, modified periodograms. *IEEE Transactions on Audio and Electroacoustics*, **15**(2), 70–73, https://doi.org/10.1109/TAU.1967.1161901.

Wilson, R., F. Dalaudier, and H. Luce, 2011: Can one detect small-scale turbulence from standard meteorological radiosondes. *Atmospheric Measurement Techniques*, **4**, 795–804, https://doi.org/10.5194/amt-4-795-2011.

Wu, X. Q., G. Sun, N. Q. Weng, L. M. Xiao, L. M. Xu, W. Y. Lü, A. L. Xu, and Q. Nie, 2007: Measurement and modeling of C^2_n at typical regions in China. *Journal of Atmospheric and Environmental Optics*, **2**, 409–422, https://doi.org/10.3969/j.issn.1673-6141.2007.06.002. (in Chinese with English abstract)